A meshless method based on moving Kriging interpolation for a two-dimensional time-fractional diffusion equation*

Ge Hong-Xia(葛红霞)[a)†] and Cheng Rong-Jun(程荣军)[b)]

[a)] *Faculty of Maritime and Transportation, Ningbo University, Ningbo* 315211, *China*
[b)] *Ningbo Institute of Technology, Zhejiang University, Ningbo* 315100, *China*

(Received 10 August 2013; revised manuscript received 8 October 2013; published online 20 February 2014)

Fractional diffusion equations have been the focus of modeling problems in hydrology, biology, viscoelasticity, physics, engineering, and other areas of applications. In this paper, a meshfree method based on the moving Kriging interpolation is developed for a two-dimensional time-fractional diffusion equation. The shape function and its derivatives are obtained by the moving Kriging interpolation technique. For possessing the Kronecker delta property, this technique is very efficient in imposing the essential boundary conditions. The governing time-fractional diffusion equations are transformed into a standard weak formulation by the Galerkin method. It is then discretized into a meshfree system of time-dependent equations, which are solved by the standard central difference method. Numerical examples illustrating the applicability and effectiveness of the proposed method are presented and discussed in detail.

Keywords: meshless method, moving Kriging interpolation, time-fractional diffusion equation

PACS: 02.60.Lj, 03.65.Ge **DOI:** 10.1088/1674-1056/23/4/040203

1. Introduction

Increasing interest has focused on the description of physical and chemical processes by means of equations involving fractional derivatives over the last few decades. Fractional partial differential equations provide a powerful tool for describing the memory and hereditary properties of different substances. Fractional derivatives are often used to model anomalous diffusion. The fractional-differential equations play an important role in modeling a number of physical phenomena and have been the focus of physics, hydrology, biology, damping laws, fluid mechanics, viscoelasticity, engineering, modeling of earth quakes, etc.[1–3]

Consequently, much attention has been paid to the solutions of fractional partial differential equations. Unfortunately, in many cases, the fractional differential equation has no analytical solution, so approximation and numerical techniques are very important and necessary. Some techniques have been developed and employed to obtain the appropriate solutions of these equations as per their physical nature. Numerical methods of solving the time fractional diffusion equations have been presented, including the Laplace transform method,[4] variation iteration method and homotopy perturbation method,[5] implicit finite difference approximation,[6] Chebyshev polynomials and finite difference method,[7] Crank–Nicolson finite difference method,[8] collocation method with radial basis functions,[9] implicit algorithm based on quadrature formula approach,[10] finite element method,[11] approximate analytical solution,[12] alternating direction implicit (ADI) approach,[13] element-free Galerkin (EFG) method,[14] and finite difference method.[15–21]

Therefore, a numerical computational method emerges as an alternative way of finding an approximate solution. In recent years, the meshless methods have developed, where a set of scattered nodes in the domain is used instead of a set of "elements" or "mesh" as in the finite element method (FEM). The meshless or meshfree methods do not require the problem domain to be discretized with meshes, and the approximate function is constructed entirely based on a set of scattered nodes. Therefore, the meshless methods can avoid the disadvantages of mesh-based methods, e.g., the FEM and the boundary element method (BEM). Many meshless methods have been developed such as the smooth particle hydrodynamics (SPH),[22] the element-free Galerkin (EFG) method,[23] the diffuse element method (DEM),[24] the reproducing kernel particle method (RKPM),[25] the meshless local Petrov–Galerkin method (MLPG),[26] the hp-meshless cloud method,[27] kp-Ritz method,[28–30] boundary element-free method (BEFM),[31,32] the complex variable meshless method,[33] etc. Meshless methods have been widely used in various fields.[34–48]

Imposing essential boundary conditions is an important and key issue in meshfree methods for lacking the Kronecker delta property, therefore, the imposition of prescribed values is not so straightforward as in the FEM. Many techniques have

*Project supported by the National Natural Science Foundation of China (Grant No. 11072117), the Natural Science Foundation of Ningbo City, China (Grant No. 2013A610103), the Natural Science Foundation of Zhejiang Province, China (Grant No. Y6090131), the Disciplinary Project of Ningbo City, China (Grant No. SZXL1067), and the K. C. Wong Magna Fund in Ningbo University, China.

†Corresponding author. E-mail: gehongxia@nbu.edu.cn

© 2014 Chinese Physical Society and IOP Publishing Ltd

been proposed, such as Lagrange multipliers, penalty method, or coupling with the FEM, etc. The Kriging interpolation technique named by a South African mining engineer Krige, is a form of generalized linear regression for the formulation of an optimal estimator in a minimum mean square error sense.[49] Gu *et al.*[50] first proposed the moving Kriging (MK) interpolation and successfully demonstrated the effectiveness of the MK interpolation functions in solving steady-state heat conduction problems. It is also found that the MK interpolation possesses a Kronecker delta function and has a consistency property.

In the present paper, a meshless method based on the MK technique for solving a two-dimensional time-fractional diffusion equation is presented. In this method, the MK technique is used to construct shape functions which possess the Kronecker delta function property and thus make it easy to implement essential boundary conditions. The governing time-fractional diffusion equations are transformed into a standard weak formulation by the Galerkin method. Numerical examples illustrating the applicability and effectiveness of the proposed method are presented and discussed in detail.

2. MK shape function

The Kriging method is a form of generalized linear regression for the formulation of an optimal estimator in a minimum mean square error sense. It has been widely used in geostatistics. We introduce the formulation of the construction of the meshless shape function by Kriging interpolation.[49,50] The MK interpolation technique is similar to the moving least-square (MLS) approximation. Assume that a problem domain Ω bounded by boundaries Γ is represented by a set of scattered nodes x_i $(i=1,2,\ldots,N)$. For estimating the value of an arbitrary field function $u(x)$ defined within Ω at a point x_0, the support domain $\Omega_{\rm S}$ ($\Omega_{\rm S}\subset\Omega$) of this point is created according to the influenced domain associated with each node. The MK interpolation is usually defined as

$$u^{\rm h}(\boldsymbol{x})=\sum_{j=1}^{m}p_j(\boldsymbol{x})a_j(\boldsymbol{x})+\boldsymbol{Z}(\boldsymbol{x})\equiv\boldsymbol{p}(\boldsymbol{x})\boldsymbol{a}(\boldsymbol{x})+\boldsymbol{Z}(\boldsymbol{x}), \quad (1)$$

where $\boldsymbol{p}_j(\boldsymbol{x})$ are monomial basis functions, $\boldsymbol{a}_j$ are monomial coefficients, and $\boldsymbol{Z}(\boldsymbol{x})$ is assumed to embody a stochastic process with mean zero, variance σ^2, and non-zero covariance. The covariance matrix of $\boldsymbol{Z}(\boldsymbol{x})$ is given by

$$\operatorname{cov}\left\{\boldsymbol{Z}(\boldsymbol{x}_i),\boldsymbol{Z}(\boldsymbol{x}_j)\right\}=\sigma^2\boldsymbol{R}[R(x_i,x_j)], \quad (2)$$

where σ^2 is a scale factor, $\boldsymbol{R}[R(\boldsymbol{x}_i,\boldsymbol{x}_j)]$ is the correlation matrix, and $R(\boldsymbol{x}_i,\boldsymbol{x}_j)$ is the correlation function between any pair of nodes located at $\boldsymbol{x}_i$ and $\boldsymbol{x}_j$. Many functions can be used as a correlation function $R(\boldsymbol{x}_i,\boldsymbol{x}_j)$, however, a simple and frequently used correlation function is the Gaussian function

$$R(\boldsymbol{x}_i,\boldsymbol{x}_j)=\exp(-\theta r_{ij}^2), \quad (3)$$

where $r_{ij}=\left\|\boldsymbol{x}_i-\boldsymbol{x}_j\right\|$, and $\theta>0$ represents a value of the correlation parameter used to fit the model. With the implementation of the best linear unbiased (BLUP),[36] equation (1) can be rewritten as follows:

$$u^{\rm h}(\boldsymbol{x})=p^{\rm T}(\boldsymbol{x})\bar{\boldsymbol{\beta}}+\boldsymbol{r}^{\rm T}(x)\boldsymbol{R}^{-1}(\boldsymbol{u}-\boldsymbol{p}\bar{\boldsymbol{\beta}}), \quad (4)$$

where

$$\bar{\boldsymbol{\beta}}=\left(\boldsymbol{P}^{\rm T}\boldsymbol{R}^{-1}\boldsymbol{P}\right)^{\rm T}\boldsymbol{P}\boldsymbol{R}^{-1}\boldsymbol{u}, \quad (5)$$

$$\boldsymbol{p}^{\rm T}(\boldsymbol{x})=\left(p_1(\boldsymbol{x}),p_2(\boldsymbol{x}),\ldots,p_m(\boldsymbol{x})\right), \quad (6)$$

$$\boldsymbol{P}=\begin{bmatrix}p_1(\boldsymbol{x}_1)&p_2(\boldsymbol{x}_1)&\cdots&p_m(\boldsymbol{x}_1)\\p_1(\boldsymbol{x}_2)&p_2(\boldsymbol{x}_2)&\cdots&p_m(\boldsymbol{x}_2)\\\vdots&\vdots&\ddots&\vdots\\p_1(\boldsymbol{x}_n)&p_2(\boldsymbol{x}_n)&\cdots&p_m(\boldsymbol{x}_n)\end{bmatrix}, \quad (7)$$

$$\boldsymbol{R}[R(\boldsymbol{x}_i,\boldsymbol{x}_j)]=\begin{bmatrix}1&R(\boldsymbol{x}_1,\boldsymbol{x}_2)&\cdots&R(\boldsymbol{x}_1,\boldsymbol{x}_n)\\R(\boldsymbol{x}_2,\boldsymbol{x}_1)&1&\cdots&R(\boldsymbol{x}_2,\boldsymbol{x}_n)\\\vdots&\vdots&\ddots&\vdots\\R(\boldsymbol{x}_n,\boldsymbol{x}_1)&R(\boldsymbol{x}_n,\boldsymbol{x}_2)&\cdots&1\end{bmatrix}, \quad (8)$$

$$\boldsymbol{r}^{\rm T}=\left(R(\boldsymbol{x}_1,\boldsymbol{x}),R(\boldsymbol{x}_2,\boldsymbol{x}),\ldots,R(\boldsymbol{x}_n,\boldsymbol{x})\right). \quad (9)$$

For simplicity, denote

$$\boldsymbol{A}=\left(\boldsymbol{P}^{\rm T}\boldsymbol{R}^{-1}\boldsymbol{P}\right)^{\rm T}\boldsymbol{P}\boldsymbol{R}^{-1}, \quad (10)$$

$$\boldsymbol{B}=\boldsymbol{R}^{-1}\left(\boldsymbol{I}-\boldsymbol{P}\boldsymbol{A}\right), \quad (11)$$

where $\boldsymbol{I}$ is an $n\times n$ unit matrix.

Equation (4) can be rewritten as

$$\begin{aligned}u^{\rm h}(\boldsymbol{x})&=\boldsymbol{p}^{\rm T}(\boldsymbol{x})\boldsymbol{A}\boldsymbol{u}+\boldsymbol{r}^{\rm T}(x)\boldsymbol{B}\boldsymbol{u}=(\boldsymbol{p}^{\rm T}(\boldsymbol{x})\boldsymbol{A}+\boldsymbol{r}^{\rm T}(\boldsymbol{x})\boldsymbol{B})\boldsymbol{u}\\&=\sum_{i=1}^{n}\boldsymbol{\Phi}_i(\boldsymbol{x})u_i=\boldsymbol{\Phi}\boldsymbol{u}, \quad (12)\end{aligned}$$

with the shape function being

$$\boldsymbol{\Phi}_i(\boldsymbol{x})=\sum_{j=1}^{m}p_j(\boldsymbol{x})A_{ji}+\sum_{j=1}^{n}r_jB_{ji}. \quad (13)$$

The partial derivatives of shape function can be easily obtained as

$$\boldsymbol{\Phi}_{i,x}(\boldsymbol{x})=\sum_{j=1}^{m}p_{j,x}(\boldsymbol{x})A_{ji}+\sum_{j=1}^{n}r_{j,x}B_{ji}, \quad (14)$$

$$\boldsymbol{\Phi}_{i,y}(\boldsymbol{x})=\sum_{j=1}^{m}p_{j,y}(\boldsymbol{x})A_{ji}+\sum_{j=1}^{n}r_{j,y}B_{ji}. \quad (15)$$

3. Meshless MK formulation for time fractional diffusion equation

Consider the following time fractional partial equation:

$$\begin{aligned}\frac{\partial u^{\alpha}(x,y,t)}{\partial t^{\alpha}}&=a(x,y,t)\frac{\partial^2u(x,y,t)}{\partial x^2}\\&\quad+b(x,y,t)\frac{\partial^2u(x,y,t)}{\partial y^2}+f(x,y,t) \quad (16)\end{aligned}$$

with the boundary condition and initial condition being as follows:

$$u(x,y,0)=\varphi(x,y),\quad (x,y)\in\Omega, \tag{17}$$

$$u(x,y,t)\,|_{\Gamma}=0,\quad 0\le t\le T, \tag{18}$$

where $\Omega=\{(x,y)\,|0\le x\le L, 0\le y\le M\}$, $\Gamma=\partial\Omega$, $0<\alpha\le 1$ is Caputo fractional-order derivative, $a(x,y,t)>0$, $b(x,y,t)>0$, $0<t\le T$.

The Caputo fractional-order derivative $\partial^{\alpha}u(x,y,t)/\partial t^{\alpha}$ is defined as

$$\begin{aligned}\frac{\partial^{\alpha}u(x,y,t)}{\partial t^{\alpha}} &= {}_{0}^{c}D_{t}^{\alpha}u(x,y,\mathrm{t})\\ &= \frac{1}{\Gamma(1-\alpha)}\int_{0}^{t}\frac{\partial u(x,y,s)}{\partial s}\frac{\mathrm{d}s}{(t-s)^{\alpha}},\\ &\quad 0<\alpha\le 1.\end{aligned} \tag{19}$$

When $\alpha=1$, equation (16) becomes a standard diffusion equation.

By taking variation and the subsection integration of Eq. (16), we obtain

$$\begin{aligned}&\int_{\Omega}\delta u\frac{\partial u^{\alpha}}{\partial t^{\alpha}}\mathrm{d}\Omega+\int_{\Omega}a(x,y,t)\frac{\partial(\delta u)}{\partial x}\frac{\partial u}{\partial x}\mathrm{d}\Omega\\ &+\int_{\Omega}b(x,y,t)\frac{\partial(\delta u)}{\partial y}\frac{\partial u}{\partial y}\mathrm{d}\Omega-\int_{\Omega}\delta uf\,\mathrm{d}\Omega=0.\end{aligned} \tag{20}$$

To establish the numerical approximation scheme, we define $\Delta x>0$ as the grid size in the x direction, $\Delta x=(b-a)/N_x$, with $x_i=a+i\Delta x$, $i=0,1,2,3,\ldots,N_x$, and $\Delta y>0$ as the grid size in the y direction, $\Delta y=(d-c)/N_y$, with $y_j=a+j\Delta x$, $j=0,1,2,3,\ldots,N_y$, and $a\le x\le b$, $c\le y\le d$ is the problem domain. The grid points in the time interval $[0,T]$ are denoted as $t_n=n\Delta t$, $n=0,1,2,3,\ldots$, where Δt is the time interval. We first give the approximation of $\partial^{\alpha}u(x,y,t)/\partial t^{\alpha}$ by a simple quadrature formula $(0<\alpha<1)$

$$\begin{aligned}&\frac{\partial^{\alpha}u(x,y,t_{n+1})}{\partial t^{\alpha}}\\ &=\frac{1}{\Gamma(1-\alpha)}\int_{0}^{t_{n+1}}\frac{\partial u(x,y,s)}{\partial s}\frac{\mathrm{d}s}{(t_{n+1}-s)^{\alpha}}\\ &=\frac{1}{\Gamma(1-\alpha)}\sum_{j=0}^{n}\left(\frac{u(x,y,t_{j+1})-u(x,y,t_j)}{\Delta t}+O(\Delta t)\right)\\ &\quad\times\int_{t_j}^{t_{j+1}}\frac{\mathrm{d}s}{(t_{n+1}-s)^{\alpha}}\\ &=\frac{1}{\Gamma(1-\alpha)}\sum_{j=0}^{n}\left(\frac{u(x,y,t_{n-j+1})-u(x,y,t_{n-j})}{\Delta t}+O(\Delta t)\right)\\ &\quad\times\int_{t_{n-j}}^{t_{n-j+1}}\frac{\mathrm{d}s}{t^{\alpha}}\\ &=\frac{1}{\Gamma(2-\alpha)}\sum_{j=0}^{n}\left(\frac{u(x,y,t_{n-j+1})-u(x,y,t_{n-j})}{(\Delta t)^{\alpha}}\right)\\ &\quad\times\left[(j+1)^{1-\alpha}-j^{1-\alpha}\right]+O\left((\Delta t)^{2-\alpha}\right)\\ &=Aa\left[u(x,y,t_{n+1})-u(x,y,t_n)\right]+Aa\sum_{j=1}^{n}Ba(j)\\ &\quad\times\left[u(x,y,t_{n-j+1})-u(x,y,t_{n-j})\right]+O\left((\Delta t)^{2-\alpha}\right),\end{aligned} \tag{21}$$

where $Aa=\left(\Gamma(2-\alpha)(\Delta t)^{\alpha}\right)^{-1}$, $Ba(j)=(j+1)^{1-\alpha}-j^{1-\alpha}$, and $\Gamma(\cdot)$ is the gamma function.

With Eqs. (12) and (21), we can obtain the approximate test functions as follows:

$$u^{\mathrm{h}}(x,y,t)=\sum_{I=1}^{n}\Phi_I(x,y)\cdot u_I(t)=\boldsymbol{\Phi}(x,y)\cdot U(t), \tag{22}$$

$$\begin{aligned}\frac{\partial u^{\mathrm{h}}(x,y,t)}{\partial x}&=\frac{\partial}{\partial x}\sum_{I=1}^{n}\Phi_I(x,y)\cdot u_I(t)\\ &=\sum_{I=1}^{n}\Phi_{I,x}(x,y)\cdot u_I(t)=\boldsymbol{\Phi}_x(x,y)\boldsymbol{U}(t),\end{aligned} \tag{23}$$

$$\begin{aligned}\frac{\partial u^{\mathrm{h}}(x,y,t)}{\partial y}&=\frac{\partial}{\partial y}\sum_{I=1}^{n}\Phi_I(x,y)\cdot u_I(t)\\ &=\sum_{I=1}^{n}\Phi_{I,y}(x,y)\cdot u_I(t)=\boldsymbol{\Phi}_y(x,y)\boldsymbol{U}(t),\end{aligned} \tag{24}$$

$$\begin{aligned}\frac{\partial^{\alpha}u^{\mathrm{h}}(x,y,t)}{\partial t^{a}}&=\boldsymbol{\Phi}(x,y)\left[Aa\left(\boldsymbol{U}(t_{n+1})-\boldsymbol{U}(t_n)\right)\right.\\ &\quad\left.+Aa\sum Ba(j)\left(\boldsymbol{U}(t_{n-j+1})-\boldsymbol{U}(t_{n-j})\right)\right],\end{aligned} \tag{25}$$

where

$$\boldsymbol{\Phi}(x,y)=(\Phi_1(x,y),\Phi_2(x,y),\ldots,\Phi_n(x,y)), \tag{26}$$

$$\boldsymbol{U}(t)=(u_1(t),u_2(t),\ldots,u_n(t))^{\mathrm{T}}, \tag{27}$$

$$\boldsymbol{\Phi}_x(x,y)=(\Phi_{1,x}(x,y),\Phi_{2,x}(x,y),\ldots,\Phi_{n,x}(x,y)), \tag{28}$$

$$\boldsymbol{\Phi}_y(x,y)=(\Phi_{1,y}(x,y),\Phi_{2,y}(x,y),\ldots,\Phi_{n,y}(x,y)). \tag{29}$$

Substituting Eqs. (22)–(25) into Eq. (20) yields

$$\delta\boldsymbol{U}^{\mathrm{T}}\boldsymbol{C}\left[\boldsymbol{Aa}\left(\boldsymbol{U}_{n+1}-\boldsymbol{U}_n\right)+\boldsymbol{D}\right]+\delta\boldsymbol{U}^{\mathrm{T}}\boldsymbol{K}\boldsymbol{U}=\boldsymbol{Q}, \tag{30}$$

where

$$\boldsymbol{U}_n=\left[u_1(t_n),u_2(t_n),\ldots,u_N(t_n)\right]^{\mathrm{T}},\quad t_n=n\cdot\Delta t, \tag{31}$$

$$\boldsymbol{C}=\int_{\Omega}\boldsymbol{\Phi}^{\mathrm{T}}(x,y)\boldsymbol{\Phi}(x,y)\mathrm{d}\Omega, \tag{32}$$

$$\begin{aligned}\boldsymbol{K}&=a(\boldsymbol{x},y,t)\int_{\Omega}\boldsymbol{\Phi}_x^{\mathrm{T}}(x,y)\boldsymbol{\Phi}_x(x,y)\mathrm{d}\Omega\\ &\quad+b(x,y,t)\int_{\Omega}\boldsymbol{\Phi}_y^{\mathrm{T}}(x,y)\boldsymbol{\Phi}_y(x,y)\mathrm{d}\Omega,\end{aligned} \tag{33}$$

$$\boldsymbol{Q}=\int_{\Omega}\boldsymbol{\Phi}^{\mathrm{T}}(x,y)f(x,y,t)\mathrm{d}\Omega, \tag{34}$$

$$\boldsymbol{D}=\boldsymbol{Aa}\sum_{j=1}^{n}\boldsymbol{Ba}(j)\left(\boldsymbol{U}_{n-j+1}-\boldsymbol{U}_{n-j}\right). \tag{35}$$

Since $\delta\boldsymbol{U}$ is arbitrary in Eq. (30), it becomes

$$\boldsymbol{C}\left[\boldsymbol{Aa}\left(\boldsymbol{U}_{n+1}-\boldsymbol{U}_n\right)+\boldsymbol{D}\right]+\boldsymbol{K}\boldsymbol{U}=\boldsymbol{Q}. \tag{36}$$

Making the time discretization of Eq. (36) by using the time central difference method, we obtain

$$\boldsymbol{C}\left[\boldsymbol{Aa}\left(\boldsymbol{U}_{n+1}-\boldsymbol{U}_n\right)+\boldsymbol{D}\right]$$

$$+\boldsymbol{K}\frac{\boldsymbol{U}_{n+1}+\boldsymbol{U}_n}{2}-\frac{\boldsymbol{Q}_{n+1}+\boldsymbol{Q}_n}{2}=0. \tag{37}$$

Now we can obtain the discrete equations about $\boldsymbol{U}_{n+1}$ as

$$\psi\boldsymbol{U}_{n+1}=\boldsymbol{\rho}\boldsymbol{U}_n+\boldsymbol{\eta}, \tag{38}$$

where

$$\psi=\boldsymbol{C}\boldsymbol{A}\boldsymbol{a}+\frac{\boldsymbol{K}}{2}, \tag{39}$$

$$\boldsymbol{\rho}=\boldsymbol{C}\boldsymbol{A}\boldsymbol{a}-\frac{\boldsymbol{K}}{2}, \tag{40}$$

$$\boldsymbol{\eta}=\frac{\boldsymbol{Q}_{n+1}+\boldsymbol{Q}_n}{2}-\boldsymbol{C}\cdot\boldsymbol{D}. \tag{41}$$

Due to the fact that MK shape functions possess the delta function property, the essential boundary conditions can be imposed easily as in the finite element method. By solving the above iteration equation, the numerical solution of a time fractional diffusion equation by the meshless MK interpolation method could be obtained.

4. Numerical results

In order to validate the present meshless MK method of solving a two-dimensional time-fractional diffusion equation, numerical examples are studied. A regular arrangement of nodes and the background meshes of cells are used for numerical integrations to solve the equation system.

4.1. Example 1

Consider the following time-fractional diffusion equation:

$$\frac{\partial u^{\alpha}(x,y,t)}{\partial t^{\alpha}}=\frac{2t^{1.6}}{\pi^2\Gamma(0.6)}\frac{\partial^2 u(x,y,t)}{\partial x^2}+\frac{t^{1.6}}{12\pi^2\Gamma(0.6)}\frac{\partial^2 u(x,y,t)}{\partial y^2}+f(x,y,t) \tag{42}$$

with boundary conditions

$$u(x,y,t)\,|_{\partial\Omega}=0 \tag{43}$$

and initial condition

$$u(x,y,0)=\sin\pi x\sin\pi y,\quad 0\le x,y\le 1 \tag{44}$$

with

$$f(x,y,t)=\frac{25t^{1.6}}{12\Gamma(0.6)}\left(t^2+2\right)\sin\pi x\sin\pi y. \tag{45}$$

The exact solution is

$$u(x,y,t)=\left(t^2+1\right)\sin\pi x\sin\pi y. \tag{46}$$

The meshless MK method is used for solving the above equation with time step length $\Delta t=0.01$, $d_{\max}=2.5$, $\alpha=0.4$. The weight function is chosen to be cubic spline and the bases are chosen to be linear. Figure 1 depicts the numerical and exact solutions at the location $x=0.2$ at $t=0.5$, 1, 1.5, and 2, respectively. The surfaces of the numerical solution with the presented method and exact solution are plotted in Figs. 2–5 at $t=0.5$, 1, 1.5, and 2, respectively. The maximum errors of different number nodes with a fixed time step are shown in Table 1. From Table 1 it follows that the errors decrease with the decrease of time step length Δt. The maximum errors of a fixed time step with different numbers of nodes are shown in Table 2. From Table 2, it can be seen that the error decreases with the increase of the number of nodes. We also compare these results from the presented method with the numerical results from the EFG method. It shows the Kriging interpolation has a sufficient advantage and a high constructing accuracy.

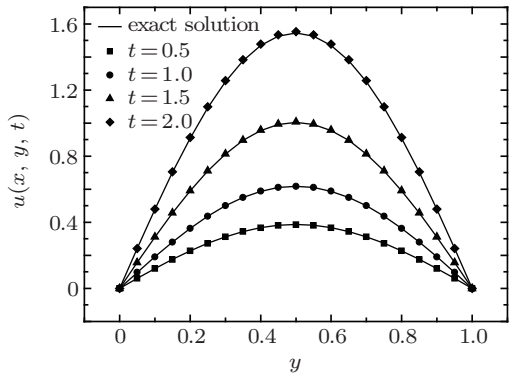


Fig. 1. Numerical solutions and exact solutions of $u(x,y,t)$ when $t=0.5$, 1, 1.5, 2 and $x=0.2$ (Example 1).

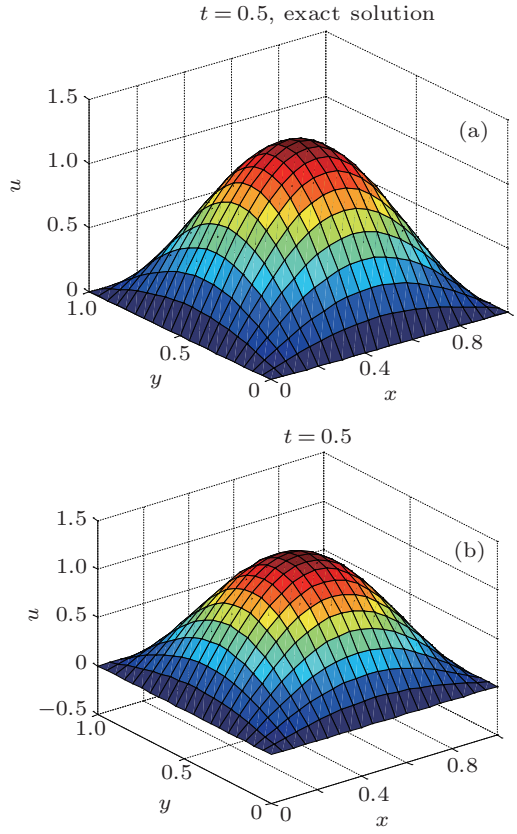


Fig. 2. (color online) Surfaces of exact (a) and numerical (b) solutions with the meshless MK method at $t=0.5$ (Example 1).

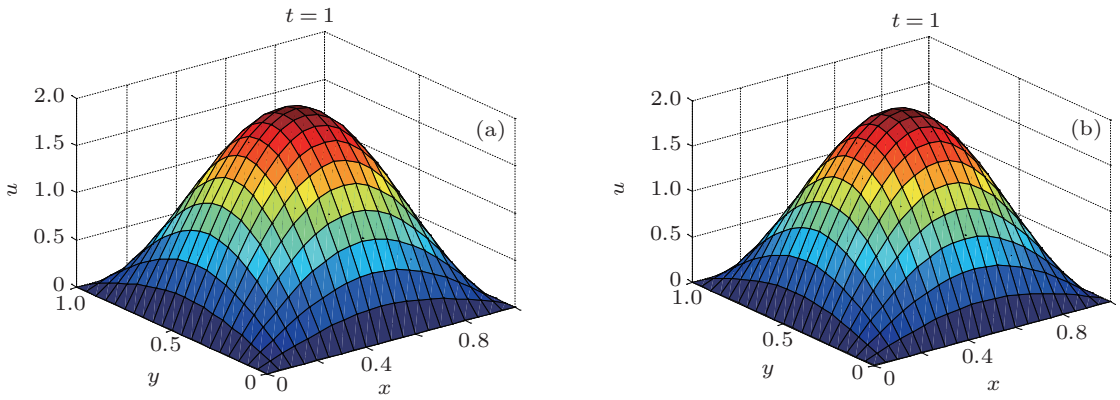


Fig. 3. (color online) Surfaces of exact (a) and numerical (b) solution with the meshless MK method at $t = 1$ (Example 1).

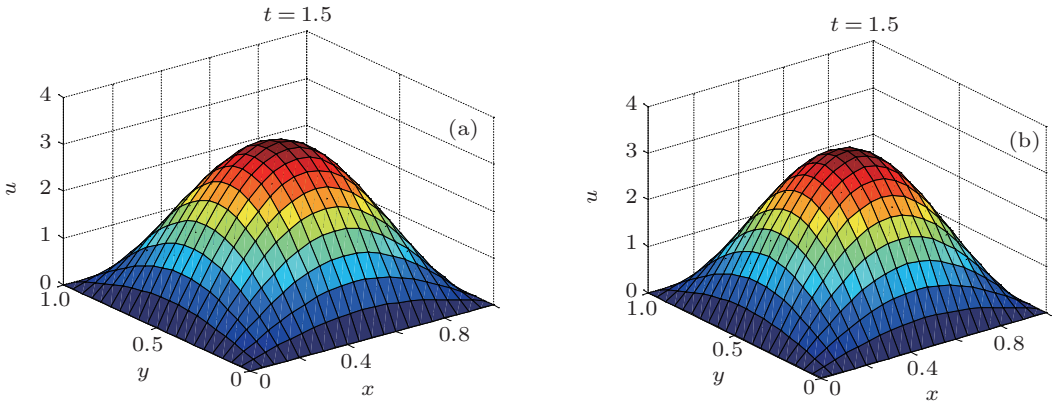


Fig. 4. (color online) Surfaces of exact (a) and numerical (b) solutions with the meshless MK method at $t = 1.5$ (Example 1).

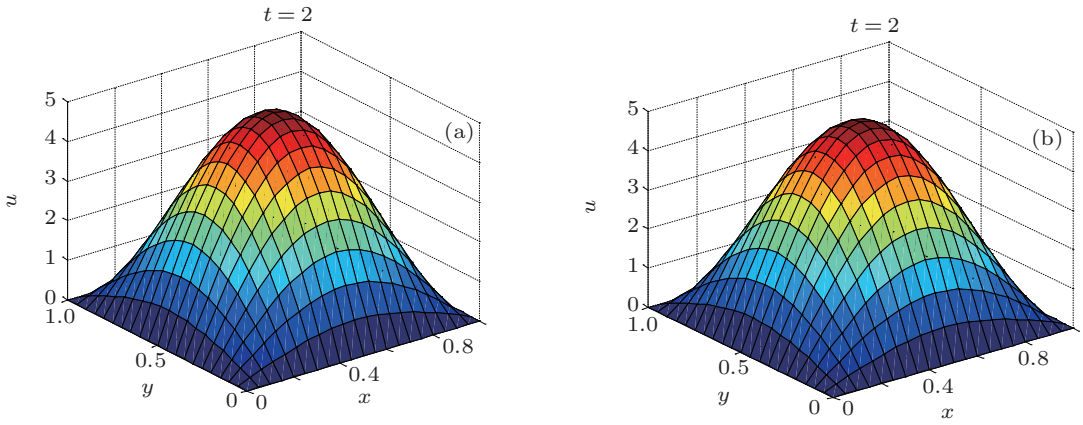


Fig. 5. (color online) Surfaces of exact (b) and numerical (b) solutions with the meshless MK method at $t = 2$ (Example 1).

Table 1. Maximum errors for the numerical solution using the presented method with a fixed number of nodes at $t = 1$.

Δt	Maximum error presented method	Maximum error EFG method
0.1	5.895×10^{-2}	6.654×10^{-2}
0.01	1.356×10^{-3}	2.373×10^{-2}
0.001	4.512×10^{-4}	3.874×10^{-3}

Table 2. Maximum errors for the numerical solution using the presented method with a fixed time step $\Delta t = 0.01$ at $t = 0.5$.

Nodes number	Maximum error presented method	Maximum error EFG method
12×12	8.317×10^{-2}	1.732×10^{-1}
21×21	1.289×10^{-3}	4.915×10^{-2}
35×35	6.242×10^{-4}	7.934×10^{-3}

4.2. Example 2

Consider the following time-fractional diffusion equation:

$$\frac{\partial u^{\alpha}(x,y,t)}{\partial t^{\alpha}} = \frac{\partial^2 u(x,y,t)}{\partial x^2} + \frac{\partial^2 u(x,y,t)}{\partial y^2} \tag{47}$$

with boundary conditions

$$u(x,y,t)|_{\partial\Omega} = 0 \tag{48}$$

and initial condition

$$u(x,y,0) = \sin \pi x \sin \pi y, \quad 0 \le x,y \le 1. \tag{49}$$

The meshless MK method is used to numerically solve the above equation with time step length $\Delta t = 0.001$, $d_{\max} = 2.5$. The weight function is chosen to be cubic spline and the bases are chosen to be linear. The numerical results obtained by the presented method are shown in Fig. 6. Figure 7 illustrates the behavior of the numerical solution at $t = 1$ with $\alpha = 0.6$, 0.7, 0.8, and 0.9, respectively. Figures 8–10 give the numerical simulation of the solution of Eq. (47) and compare the responses of the diffusion system at $t = 1.0$ when $\alpha = 0.6$, 0.7, 0.8, 0.9, respectively. From Figs. 7–10, it can be seen that the solution continuously depends on the time fractional derivative.

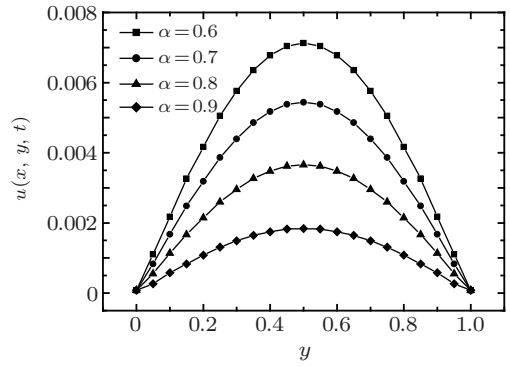


Fig. 6. Behaviors of numerical solutions at $\alpha = 0.6$, 0.7, 0.8, 0.9 at $t = 1$ and $x = 0.2$ (Example 2).

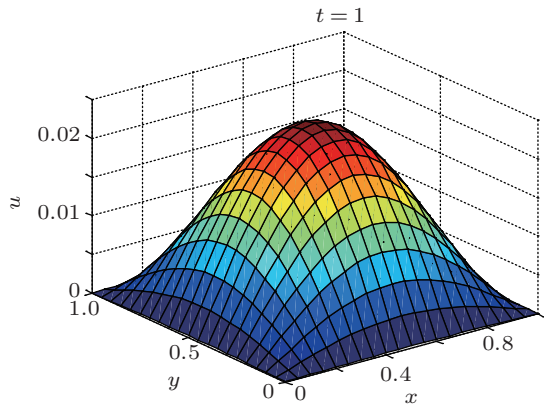


Fig. 7. (color online) Surface of the numerical solution with the meshless MK method with $\alpha = 0.6$ at $t = 1$ (Example 2).

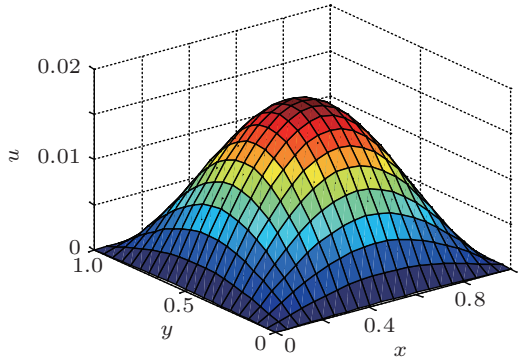


Fig. 8. (color online) Surface of the numerical solution with the meshless MK method with $\alpha = 0.7$ at $t = 1$ (Example).

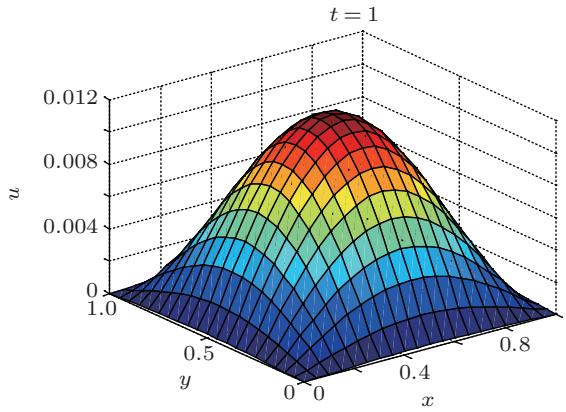


Fig. 9. (color online) Surface of the numerical solution with the meshless MK method with $\alpha = 0.8$ at $t = 1$ (Example 2).

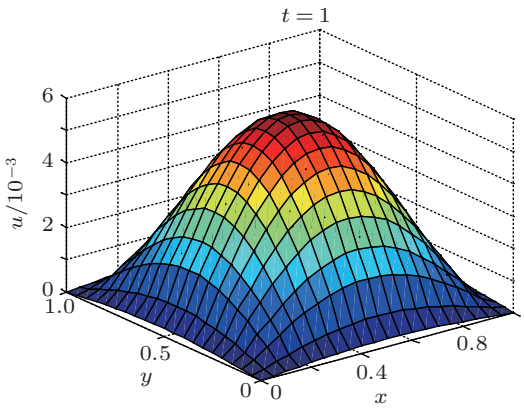


Fig. 10. (color online) Surface of the numerical solution with the meshless MK method with $\alpha = 0.9$ at $t = 1$ (Example 2).

From these numerical results it follows that the presented method of solving the time-fractional diffusion equation is efficient and accurate.

5. Conclusion

A successful application of the present meshless method based on MK interpolation for a two-dimensional time-fractional diffusion equation is demonstrated in this paper. By making use of the good feature of the Kronecker delta property, the presented method is effective and convenient to impose the essential boundary conditions, and the procedure is

straightforward as in the FEM. As a result, the combination of the novel MK interpolation and the element-free Galerkin method is an attractive method. Numerical results show that the present MK meshfree method is efficient, accurate, and stable for solving two-dimensional time-fractional diffusion equations. Summarizing these results, the proposed method gives a reasonable calculation and has easy-to-use features and a good potential. This method is also promising to be extended to other fractional partial differential equations and nonlinear problems. All results are obtained by using MATLAB version 7.0.

References

[1] Liu F, Shen S, Anh V and Turner I 2005 *ANZIAM J.* **46** 488
[2] Metzler R and Klafter J 2005 *Phys. Rep.* **339** 1
[3] Podlubny I 1999 *Fractional Differential Equation* (New York: Academic Press) p. 21
[4] Debnath L and Bhatta D 2004 *Frac. Calc. Appl. Anal.* **7** 21
[5] Sweilam N H, Khader M M and Al-Bar R F 2007 *Phys. Lett. A* **371** 26
[6] Murio A 2008 *Comput. Math. Appl.* **56** 1138
[7] Khader M M 2011 *Commun. Nonlinear Sci. Numer. Simul.* **16** 2535
[8] Sweilam N H, Khader M M and Mahdy A M S 2012 *J. Fract. Calc. Appl.* **2** 1
[9] Bagley R L and Torvik P J 1984 *J. Appl. Mech.* **51** 294
[10] Diethelm K 1997 *Electron. Trans. Numer. Anal.* **5** 1
[11] Enelund M and Josefson B L 1997 *AIAA J.* **35** 1630
[12] He J H 1998 *Comput. Methods Appl. Mech. Eng.* **167** 57
[13] Tadjeran C and Meerschaert M M 2007 *J. Comput. Phys.* **220** 813
[14] Ge H X, Liu Y Q and Cheng R J 2012 *Chin. Phys. B* **21** 010206
[15] Zhang Y 2009 *Appl. Math. Comput.* **215** 524
[16] Sweilama N H, Khader M M and Nagyb A M 2011 *J. Comput. Appl. Math.* **235** 2832
[17] Zhuang P and Liu F 2007 *J. Alg. Comput. Technol.* **1** 1
[18] Meerschaert M M, Scheffer H P and Tadjeran C 2006 *J. Comput. Phys.* **11** 249
[19] West B J, Bolognab M and Grigolini P 2003 *Physics of Fractal Operators* (New York: Springer) p. 12
[20] Yuste S B 2006 *J. Comput. Phys.* **216** 264
[21] Yuste B and Acedo L 2005 *SIAMJ Numer. Anal.* **42** 1862
[22] Gingold R A and Moraghan J J 1977 *Mon. Not. R. Astr. Soc.* **181** 375
[23] Belytschko T, Lu YY and Gu L 1994 *Int. J. Numer. Methods Eng.* **37** 229
[24] Nayroles B, Touzot G and Villon P 1992 *Comput. Mech.* **10** 307
[25] Liu W K, Jun S and Zhang Y F 2001 *Int. J. Numer. Methods Fluids* **20** 1081
[26] Arluri S N and Zhu T L 1998 *Comput. Mech.* **22** 117
[27] Liszka T J, Duarte C A M and Tworzydlo W W 1996 *Comput. Methods Appl. Mech. Eng.* **139** 263
[28] Cheng R J and Liew K M 2012 *Comput. Method Appl. Mech. Eng.* **245** 132
[29] Lim C W and Liew K M 1994 *J. Sound Vib.* **173** 343
[30] Liew K M and Feng Z C 2001 *Int. J. Mech. Sci.* **43** 2613
[31] Peng M J and Cheng Y M 2009 *Eng. Anal. Bound Elem.* **33** 77
[32] Cheng Y M and Peng M J 2005 *Sci. Chin. Ser. G: Phys. Mech. Astron.* **48** 641
[33] Liew K M and Cheng Y M 2009 *Comput. Methods Appl. Mech. Eng.* **198** 3925
[34] Cheng R J and Cheng Y M 2007 *Acta Phys. Sin.* **56** 5569 (in Chinese)
[35] Dai B D and Cheng Y M 2007 *Acta Phys. Sin.* **56** 597 (in Chinese)
[36] Cheng R J and Cheng Y M 2008 *Acta Phys. Sin.* **57** 6037 (in Chinese)
[37] Cheng R J and Ge H X 2009 *Chin. Phys. B* **18** 4059
[38] Wang J F, Sun F X and Cheng R J 2010 *Chin. Phys. B* **19** 060201
[39] Cheng R J and Ge H X 2010 *Chin. Phys. B* **19** 090201
[40] Cheng Y M and Li J H 2006 *Sci. China Ser. G: Phys. Mech. Astron.* **49** 46
[41] Wang J F and Cheng Y M 2011 *Chin. Phys. B* **20** 030206
[42] Cheng R J and Cheng Y M 2011 *Chin. Phys. B* **20** 070206
[43] Cheng R J and Cheng Y M 2011 *Acta Phys. Sin.* **60** 070206 (in Chinese)
[44] Cheng R J and Ge H X 2012 *Chin. Phys. B* **21** 040203
[45] Cheng R J and Ge H X 2012 *Chin. Phys. B* **21** 100209
[46] Cheng R J and Liew K M 2014 *Appl. Math. Comput.* **227** 274
[47] Cheng R J and Wei Q 2013 *Chin. Phys. B* **22** 060209
[48] Shi T Y, Cheng R J and Ge H X 2013 *Chin. Phys. B* **22** 060210
[49] Krige D G 1976 *Advanced Geostatistics in the Mining Industry* **23** 279
[50] Gu L 2003 *Int. J. Numer. Methods Eng.* **56** 1